Catalysis Today 282 (2017) 111–122

Contents lists available at ScienceDirect

Catalysis Today

journal homepage: www.elsevier.com/locate/cattod

# Hydrogenation of tetralin in presence of nitrogen using a noble-bimetallic couple over a Ti-modified SBA-15

Verónica A. Vallés[a], Brenda C. Ledesma[a], Gina A. Pecchi[b], Oscar A. Anunziata[a], Andrea R. Beltramone[a,*]

[a] Centro de Investigación en Nanociencia y Nanotecnología (NANOTEC), Facultad Regional Córdoba, Universidad Tecnológica Nacional, Maestro López y Cruz Roja Argentina, 5016, Córdoba, Argentina
[b] Departamento Físico-Química, Facultad de Ciencias Químicas, Universidad Concepción, Concepción, Chile

ARTICLE INFO

*Article history:*
Received 19 January 2016
Received in revised form 13 June 2016
Accepted 2 July 2016
Available online 12 July 2016

*Keywords:*
Platinum-iridium
Indole
Quinoline
HDN
HYD

ABSTRACT

Monometallic Pt- and bimetallic Pt-Ir-modified Ti-SBA-15 were used in the hydrogenation of tetralin to decalin in the presence of 150 ppm of N as quinoline and indole at 250 °C and 15 atm of pressure of hydrogen, using a Parr reactor. The catalyst was synthesized using sol-gel method and Ti was added during the synthesis using Tetraethyl Orthotitanate. Pt/Ir was added by wetness impregnation. The catalysts prepared were extensively characterized by X-ray diffraction (XRD), $N_2$ adsorption isotherms, UV–vis-DRS, Raman spectroscopy, XPS, TEM-EDS and TPR. UV–vis-DRS and Raman spectroscopy confirmed that Ti was incorporated in tetrahedral coordination in the framework of the SBA-15. The analysis showed that the mesoporous structure was maintained after metal incorporation and Ti incorporation helps to reduce significantly the size of the metals clusters and improves its dispersion considerably. Pt-Ir/Ti-SBA-15 was the most active catalyst. The experimental data were quantitatively represented by a modified Langmuir-Hinshelwood type rate equation. The preliminary results show these materials as a promising catalyst for HDT reactions.



## 1. Introduction

The increased attention paid to catalytic hydrogenation in the oil refining industry is due in part to legislation regarding the maximum contents of sulfur, aromatic compounds, and alkenes in traffic fuels [1,2]. Aromatics in diesel increase the particle emissions in exhaust gases and they have the further effect of lowering the fuel quality [2]. Alkenes in gasoline are undesired in larger amounts because of higher NOx and CO formation and the higher reactivity of evaporative emissions in comparison to their saturated counterparts.

Many factors such as the catalysts [3–11], process parameters [10–12], feedstock source and quality [13–17], reactivities of sulfur compounds [16–19], inhibition effects of $H_2S$ [20–24], nitrogen compounds [25–28] and aromatics [29–32] present in the feed can have significant influences on the degree of hydrogenation of diesel feeds. The two-stage processing strategy is now considered as a good alternative in the hydrotreating process (HDT), first stage employs a base metal catalyst, while the second stage applies high activity noble metal catalyst. Transition metals such as Rh, Ir, Ru and Pt supported on silica or alumina are known to catalyze effectively the nitrogen removal [33–38], iridium has been established as a strong promoter element for the HDN activity.

Noble metal-based catalysts have high activity for hydrogenation of aromatic hydrocarbons, and the process can then perform at low temperatures and pressures and lower contact times. However, these catalysts have a low tolerance to sulfur and nitrogen poisoning, therefore a previous deep hydrodesulfurization and hydrodenitrogenation charge pre-treatment is required. This two stage hydrodearomatization (HDA) process has a high operating cost and, consequently, the development of noble metal-based catalysts with tolerance to sulfur and nitrogen has become attractive.

Many studies describes the influence of the support on the performance of hydrotreating catalysts such as molecular sieves [39], zirconia [40] and titania [41] oxides, amorphous and ordered mesoporous silica-aluminas such as MCM-41, SBA-15, KIT-6 and FSM-16 [42–46] materials. In recent years, the mesoporous silicate materials with ordered pore structure, which have large pore diameters and high surface area, attracted widespread attention as new potential materials for the preparation of supported hydrotreating catalysts. SBA-15 is highly stable with better textural properties

* Corresponding author.
*E-mail addresses:* abeltramone@frc.utn.edu.ar, lelitajones@hotmail.com (A.R. Beltramone).

http://dx.doi.org/10.1016/j.cattod.2016.07.004
0920-5861/

compared to alumina. Substituting the foreign ions (Al3+, Ti4+, Zr4+) into the silicate framework has proven to be efficient route in order to enhance acidity and stability of the mesoporous silica. Some authors reported that Al, Ti, or Zr containing SBA-15 provided a better dispersion of Ni (Co) and Mo (W) species as compared to the pure SBA-15 and alumina supported catalysts [47–49].

In our previous work we reported the effect of the incorporation of titanium in tetrahedral position into the framework of SBA-16 mesoporous materials. Titanium provided a better dispersion of the smaller iridium metallic clusters than siliceous-SBA-16 [50]. We also investigated the hydrogenation of tetralin using a bimetallic Pt-Ir-catalysts supported in SBA-15 [51]. These studies showed high activity, selectivity and stability as well also greater resistance to poisons.

Nitrogen compounds are amongst the most difficult compounds to eliminate due to the strength of the aromatic C—N bonds involved. Is very important obtain a complete picture about the inhibiting effect from nitrogen species (i.e. the relative inhibition of basic and non-basic nitrogen compounds on HYD and HDS). Herein we have investigated the effect of basic and non-basic nitrogen compounds on HYD of tetralin under practically relevant reaction conditions. Competitive adsorption is expected to affect the hydrogenation rates [52–55]. In the present work three compounds tetralin, indole (non-bassic) and quinoline (basic-nitrogen compound) were used as models for simulating the HDN feed using a monometallic Pt- and a bimetallic Pt-Ir- supported Ti-SBA-15 as catalysts.

## 2. Experimental

### 2.1. Synthesis of Ti-SBA-15

In order to introduce titanium atoms in tetrahedral position replacing Si in the framework of SBA-15, the following proceeding was carried out: Tetraethylorthosilicate (TEOS, 98%, Sigma–Aldrich) was used as a source of Si, Tetraethylorthotitanate (TEOT, 98% Sigma–Aldrich) as a source of Ti. The template Pluronic 123 in acidic medium (9 g) was dissolved in 288 mL of HCl (2 M). The temperature of the P123 solution was controlled at 35 °C. After that, 20.1 mL of TEOS were added to the P123 solution under stirring for 20 min, and then 2.1 mL of TEOT were added to the resultant solution and maintained at static condition for 24 h. The resultant mix was transferred into a Teflon bottle and maintained at 80 °C for 24 h without stirring. The sample was calcined at 550 °C for 5 h to remove the copolymer template. This sample with Si/Ti = 10 will be referred as Ti-SBA-15.

### 2.2. Synthesis of monometallic and bimetallic supported Ti-SBA-15

Platinum nanoparticles were incorporated into Ti-SBA-15 support by the wet impregnation method. Platinum and Iridium nanoparticles were incorporated by co-impregnation in the case of the bimetallic catalyst. The metal precursors (Iridium acetylacetonate ($Ir(acac)_2$) and cloroplatinic acid ($H_2PtCl_6xH_2O$)) were dissolved in 50 mL of ethanol at 50 °C under reflux. A finely ground powder fraction of the Ti-SBA-15 was dried in static air at 120 °C for 12 h, then, it was directly incorporated to the metal precursor solution. The solution was placed in a rotary evaporator to remove excess of ethanol at about 50 °C and 60 rpm. The obtained powder was then dried at 120 °C overnight, and desorbed in inert atmosphere (nitrogen flow of 20 mL/min) from 25 °C to 470 °C with a slope of 4 °C/min and kept at 470 °C during 5 h. Then the samples were calcined at 500 °C for 5 h. Due to the metals are active for the reaction in its metallic state, the samples were reduced in $H_2$ flow of 20 mL/min at 470 °C using the same procedure described above. The total metal weight loadings were adjusted in order to have the desired metal molar fraction. Here in after these catalysts will be referred as: monometallic Pt/Ti-SBA-15 (nominal content of 1 wt.% of Pt) and bimetallic Ir-Pt/Ti-SBA-15, (nominal content of 0.5 wt.% of Pt and 0.5 wt.% of Ir).

### 2.3. Characterization of the catalysts

XRD patterns were collected by using a continuous scan mode. The scan speed was 0.02 deg (2 θ)/min in the Philips X'Pert PRO PANalytical diffractometer, operating with CuKa X-ray radiation (X-ray generator current and voltage set at 40 mA and 45 kV), using small divergence and scattering slits of 1/32 mm and a goniometer speed of $1.2^\circ(2\theta)min^{-1}$. The scanning range was set between 0.5° and 5°. The sample was crushed previously and placed in an aluminum sample holder. Elemental analysis was performed by inductively coupled plasma-atomic emission spectroscopy (VISTA-MPX) operated with high frequency emission power of 1.5 kW and plasma airflow of 12.0 L/min. TPR was performed using a Micromeritics Chemisorb 2720 apparatus, with a flow of 14 mL/min of 10 mol% of $H_2/N_2$ heating up 500 °C. $N_2$ adsorption/desorption isotherms at −196 °C were measured on ASAP 2420 from Micromeritics after degassing the samples at 400 °C, determining textural properties as surface area and pore volume, pore size distribution was estimated using Barrett, Joyner, and Halenda algorithm, with accuracy of ±2% for all measurements. The carbon monoxide chemisorption measurements were performed in ASAP 2420 equipment, after in-situ reduction with pure $H_2$ at 300 °C for 3 h. The isotherms were measured at 35 °C and torr pressure range of 0–400. Ultraviolet-visible diffuse reflectance spectroscopy (UV–vis-DRS) was used to evaluate the relative distribution of octahedrally- to tetrahedrally-coordinated Ti species in the samples. The spectra were recorded with a PerkinElmer Lamba 650 spectrophotometer equipped with a diffuse reflectance accessory. Raman spectrum was obtained from an InVia Reflex Raman microscope and spectrometer using a 532 nm diode laser excitation. X-ray Photoelectron Spectra (XPS) were obtained on a MicrotechMultilb 3000 spectrometer, equipped with a hemispherical electron analyzer and MgKα (hν = 1253.6 eV) photon source. An estimated error of ±0.1 eV can be assumed for all measurements. Peak intensity was calculated from the respective peak areas after background subtraction and spectrum fitting by a combination of Gaussian/Lorentzian functions. TEM were recorded in a JEOL 2100 F microscope operated with an accelerating voltage of 200 kV (point resolution of 0.19 nm); coupled with Energy dispersive X-ray spectroscopy (EDS). JASCO 5300 FTIR spectrometer was used for Py-FTIR measurements. A thermostated cell with a special NaBr window warmed up to 400 °C and $4.2 \times 10^{-2}$ Torr during 2 h was employed to avoid possible sample hydration.

### 2.4. Catalytic activity

The hydrogenation reaction of teteralin in presence of the N-compound was carried out at 250 °C and 15 atm of $H_2$ and 500 rpm in a 600 mL stirred autoclave (Parr Pressure Reactor 4536). The typical procedure was as follows: Tetralin was dissolved in 50 mL of dodecane to a concentration of 5 wt.%, 150 ppm of N as indole (Feed 1) or quinoline (Feed 2) were added. The mixture was poured into the autoclave and the catalyst (250 mg) was transferred to the reactor. The reaction time was 8 h; samples were taken every half an hour. The results were compared with those of a typical HDN catalyst $NiMo/Al_2O_3$ Criterion DN200. This catalyst was presulfided according to [56]. The products were analyzed with a HP 5890 Series II GC and HP-5 capillary column and identified by GC/MS.

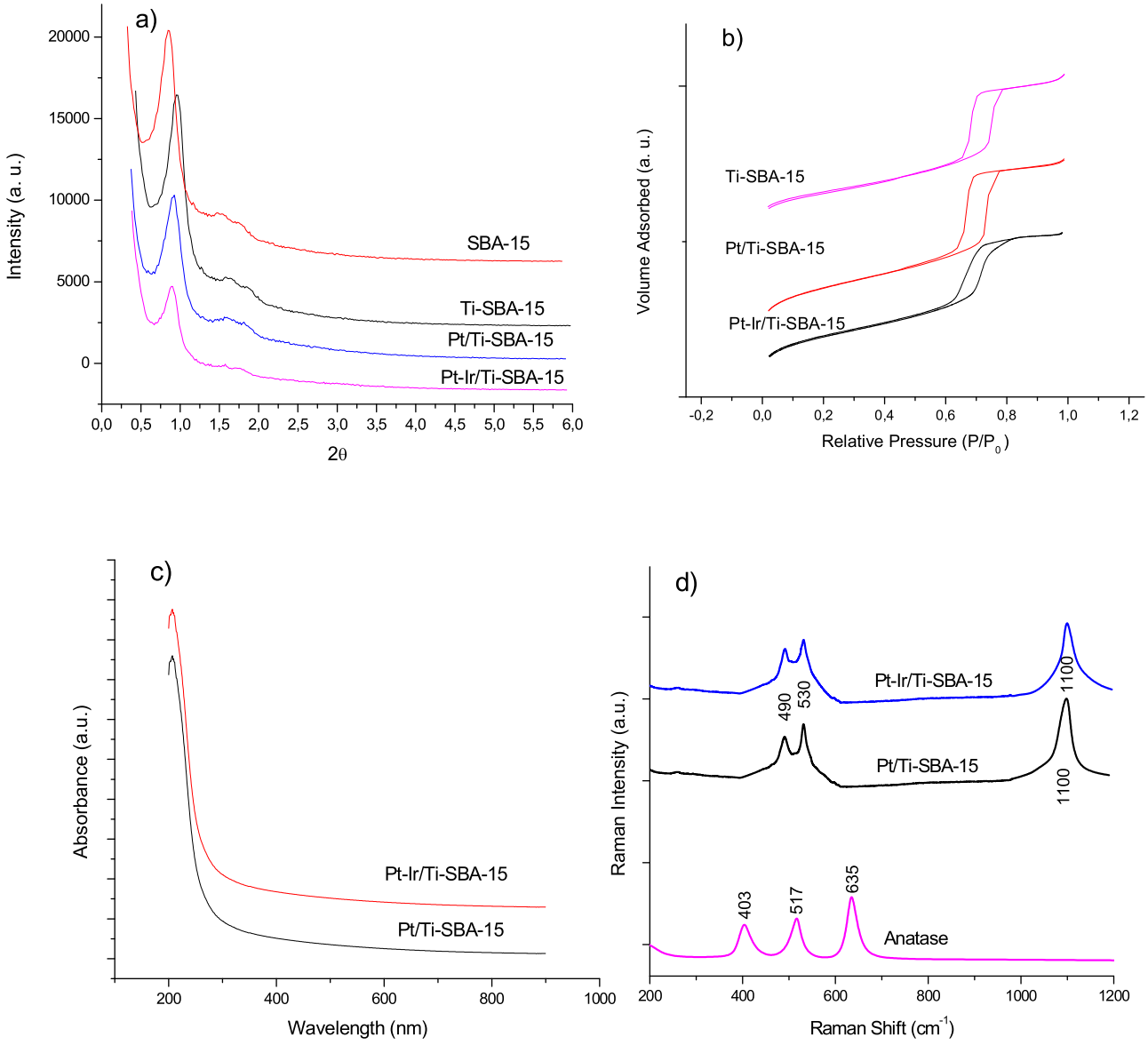


**Fig. 1.** (a) XRD pattern; (b) $N_2$ adsorption–desorption isotherms; (c) UV–vis Diffuse Reflectance Spectroscopic and (d) Raman of the samples synthesized.

## 3. Result and discussion

### 3.1. Characterization of the catalysts

#### 3.1.1. XRD, $N_2$ adsorption isotherms, UV–vis-DRS and RAMAN

Fig. 1a shows the XRD plots of the synthesized samples. Siliceous SBA-15 pattern used as reference [51] showed three-peak around $2\theta = 0.80$, 1.4 and 1.6, which are characteristic peaks of SBA-15 type mesoporous materials, representing the d100, d110 and d200 planes with 2D hexagonal order of p6 mm symmetry structure. The unit-cell parameter, $a_0$ (Table 1) of the crystallographic structure is obtained by solving an equation depending on the type of space group. For a hexagonal SBA-15 structure, where *d* is the interplanar spacing, $a_0$ is given by:

$$a_0 = 2d_{100}/(3)^{1/2} \quad (1)$$

The peak position for Ti-SBA-15 slightly shifted to higher angles. The shift of unit cell parameter may be attributed to longer Ti—O bond length compared to Si—O bond. Such an observation indicates successful incorporation of Ti into SBA-15 structure. In the wide-angle XRD pattern of the samples synthesized, between 15 and 80 2θ values (Figure not shown), the absence of characteristic peaks of anatase/rutile phase, indicates an adequate incorporation of Ti in tetrahedral position.

**Table 1**
Structural and textural properties of the catalysts.

| | SBA-15 | Pt/Ti-SBA-15 | Pt-Ir/Ti-SBA-15 |
|---|---|---|---|
| Area ($m^2$/g) | 1050 | 805 | 680 |
| $a_0$ (nm) | 12.04 | 11.5 | 10.9 |
| $d_p$ (nm) | 6.5 | 6.4 | 5.2 |
| $V_p$ ($cm^3$/g) | 1.1 | 1.09 | 0.96 |
| Ti/Si (EDS) | | 0.11 | 0.11 |
| Pt/Ir wt.% (ICP) | – | 1.08 | 0.54/0.49 |

The nitrogen adsorption-desorption isotherms (Fig. 1b) of Ti-SBA-15, Pt/Ti-SBA-15 and Pt-Ir/Ti-SBA-15 samples exhibit type IV isotherms with hysteresis loops in the relative pressure range from 0.7 to 0.80, which confirm the mesoporous nature of these materials.

The Brunauer–Emmett–Teller (BET) surface areas and the pore diameter and volume are listed in Table 1. These results indicate that the structure remains unchanged after Ti addition, in

**Table 2**
XPS Binding energies and atomic surface ratio.

| Samples | Binding energies (eV) of core levels | | | | | Atomic surface ratios | | |
|---|---|---|---|---|---|---|---|---|
| | Si2p | Ti2p | O1s | Pt4f7/2([a]) | Ir4f7/2([a]) | Ti/Si | Pt/Si | Ir/Si |
| Pt/Ti-SBA-15 | 103.4 | 459.5 | 532.9 | 71.4 ($Pt^0$ = 93)<br>73.5 ($Pt^{+2}$ = 7) | ----<br>---- | 0.0029 | 0.0011 | ---- |
| Pt-Ir/Ti-SBA-15 | 103.4 | 459.7 | 532.9 | 71.8 ($Pt^0$ = 88)<br>73.9 ($Pt^{+2}$ = 12) | 61.1 ($Ir^0$ = 89)<br>62.6 ($Ir^{+2}$ = 11) | 0.0027 | 0.0008 | 0.0007 |

[a] wt.% of Pt and Ir species ($Pt^0$, $Pt^{2+}$, $Ir^0$ and $Ir^{2+}$) in monometallic and bimetallic samples.

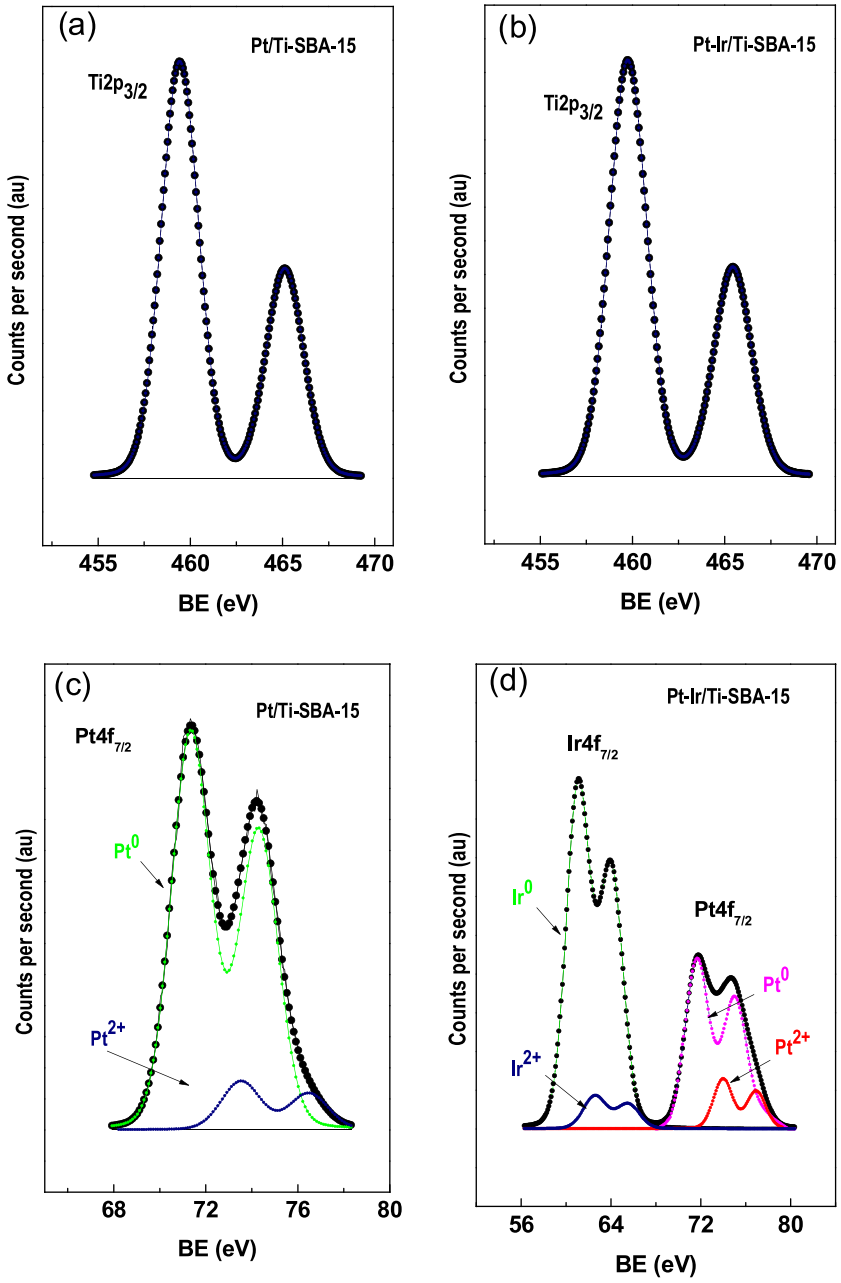


**Fig. 2.** XPS of the samples synthesized.

agreement with XRD. In all cases, the average pore size and pore volume is quite similar and slightly lower than presented by the material support, confirming that no pore blockage occurs after metal (Pt/Ir) incorporation. UV–vis diffuse reflectance spectroscopy (UV–vis–DRS) (Fig. 1c) was used to study the dispersion and chemical environment of Ti incorporated in SBA-15 matrix. Fig. 1c shows the spectra of Ti-SBA-15 after incorporation of Pt and Pt-Ir nanoclusters. The band at 210 nm, corresponding to tetragonal titanium with $Ti(OSi)_4$, structure is present in both samples. The intense ligand-to-metal charge transfer transition band at ~200 nm (between titanium and oxygen in the framework $p\pi-d\pi$) is attributed to mono-atomically dispersed $Ti^{4+}$ ions in tetra-

coordinated geometry [57–59]. The results indicate that, in these samples, the Ti species introduced are well-dispersed in the SBA-15 mesoporous framework, in good agreement with what is determined from the wide angle XRD patterns. Raman Spectroscopy of the samples is showed in Fig. 1 d, three bands are observed in Pt-Ir/Ti-SBA-15 and Pt/Ti-SBA-15 at 490, 530 and 1100 $cm^{-1}$. The signals at lower frequency correspond to bending and symmetric stretching vibration of Ti-O-Si species in the framework, respectively. The band at 1100 $cm^{-1}$ is due to the symmetric vibration of tetrahedral coordinated $[Ti(OSi)_4]$ units in SBA-15 [60]. Anatase spectrum showed is used as reference. The absence of characteristic anatase bands [61] indicates the incorporation of Ti in tetrahedral position.

### 3.1.2. XPS

According to XPS spectra (Fig. 2a and b) and Table 2, the appearance of the signal of Ti2p3/2 at 459 eV is indicative of tetrahedral Ti coordinated (NN = 4) due to isomorphous Si substitution [62]. Thus, in agreement with the data obtained by UV–vis and Raman spectroscopy, titanium is incorporated as $Ti^{+4}$ isolated ions in tetrahedral (Td) coordination.

XPS spectra and binding energies (BE) of core electrons of platinum and iridium (4f signal) are also shown in Fig. 2c and d and Table 2, respectively. According to the literature, BE at 61.0 eV is assigned to $Ir^0$ and 62.0 eV is assigned to Ir-O [63–65]. BE of Pt4f of metallic Pt, in Pt/Ti-SBA-15 appears at 71.4 eV, whereas in Pt-Ir/Ti-SBA-15 around 71.8 eV. The shift to higher BE for Pt 4f in the Pt-Ir sample could be related to a lower electron density on the Pt sites due to the presence of Ir (higher electron affinity). The shifts of the BE of Pt suggest the formation of a bimetallic Ir-Pt alloy, as reported for similar systems following the Pt4f7/2 and Ir4f7/2 peaks [63–65]. On the other hand, the diminution of Ir-O species in Ir-Pt samples indicated the electronic transfer from Pt to Ir. Peak area analysis gives a major contribution of metallic Pt and Ir; $Pt^0$ and $Ir^0$ content is more than 88% in all cases, indicating that in both samples the noble metals are metallic atoms after the reduction procedure.

According to the atomic surface composition of the samples (Table 2) at 50–100 Å of depth (external surface of the catalysts), the low atomic ratios (% at) would indicate that most of the metals are in the inner surface of the material.

### 3.1.3. TPR

The characterization of the catalysts is also carried out by temperature-programmed reduction; each spectrum provides information of the reducibility of the catalyst. TPR profiles plotted in Fig. 3 shows the reduction temperatures for the samples synthesized. Pt/SBA-15 presents only one peak at 210 °C. In the Ti-containing samples, the reduction temperature of the platinum species decreases to 175 °C, this indicates that Ti incorporation improves the reducibility of platinum. The appearance of a peak not seen in the monometal system has been used as a measure of bimetal formation [66]. In the bimetallic sample the reduction peak occurred at slightly higher temperature than that of Pt/Ti-SBA-15, this is due that iridium has higher reduction temperature than Pt. Another indication of bimetal formation that applies to the platinum-iridium system is the appearance/disappearance of the

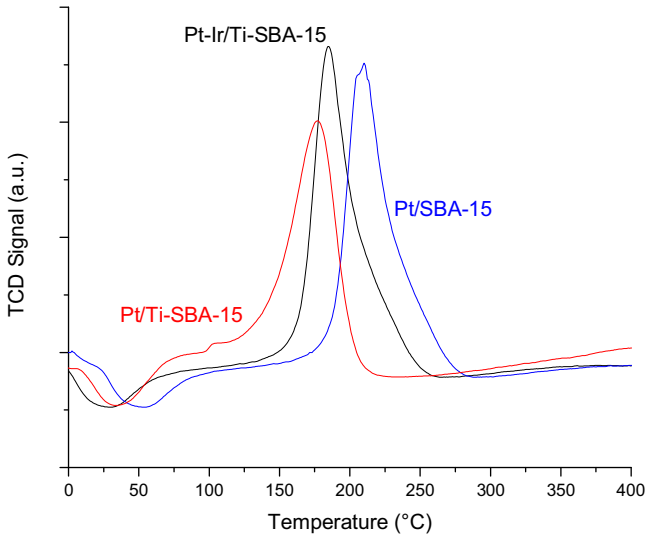


**Fig. 3.** TPR of the samples synthesized.

$IrO_2$ peak. It is known that the oxidative agglomeration of iridium to form $IrO_2$ is inhibited by platinum-iridium bimetal formation [66].Therefore the disappearance of the $IrO_2$ peak in the reduction profile can be used to identify bimetal formation. Likewise, the $IrO_2$ peak is not observed in the case of the Pt-Ir/Ti-SBA-15. The platinum-iridium bimetal formation in different supports has been investigated [67]. It has been proposed that the ease of bimetal formation varies as: $TiO_2$ (easiest) $>SiO_2 > A1_2O_3$ [67]. This is in agreement with the presence of one peak at lower temperature of the reduction indicating the formation of the Pt-Ir alloy in Pt-Ir/Ti-SBA-15 catalysts.

### 3.1.4. TEM

In Fig. 4a and b, we can observe that Ti-SBA-15 shows a typical hexagonal pore structure of SBA-15 materials with network channels, uniform pore size and long-range ordering. The calculated pore diameter was about 6 nm, close to that estimated from nitrogen sorption isotherms. No changes in morphology were observed after the modification, suggesting that the metals are uniformly dispersed on Ti-SBA-15 support.

From the TEM micrograph, the calculated metal-cluster size was about 2.5 nm for the monometallic Pt/Ti-SBA-15 (Fig. 4c) and about 3-3.5 nm for the bimetallic Pt-Ir/Ti-SBA-15 (Fig. 4d). This finding probed that Ti incorporation helped to reduce the metal cluster size and improved metal dispersion compared with our previous report on bimetallic couples supported on siliceous-SBA-15 [51]. In the case of bimetallic Pt-Ir/Ti-SBA-15, the higher size of the deposited species inside the pores could be the reason for decreasing size of the pores with the subsequent decreasing in area (Table 1). This can be due to a higher load of channels because of the larger nanoparticles, than in the monometallic catalyst.

**Table 3**
Quantification of Bronsted and Lewis sites at different temperatures.

| | SBA-15 | | Ti/SBA-15 | | Pt/Ti-SBA-15 | | Pt-Ir/Ti-SBA-15 | |
|---|---|---|---|---|---|---|---|---|
| Temperature (°C) | B (mmol/g) | L (mmol/g) | B (mmol/g) | L (mmol/g) | B (mmol/g) | L (mmol/g) | B (mmol/g) | L (mmol/g) |
| 50 | – | 0.20 | – | 0.90 | – | 0.88 | – | 0.75 |
| 100 | – | 0.12 | – | 0.46 | – | 0.51 | – | 0.45 |
| 200 | – | 0 | – | 0.12 | – | 0.10 | – | 0.08 |
| 300 | – | 0 | – | 0.03 | – | 0.00 | – | 0.00 |

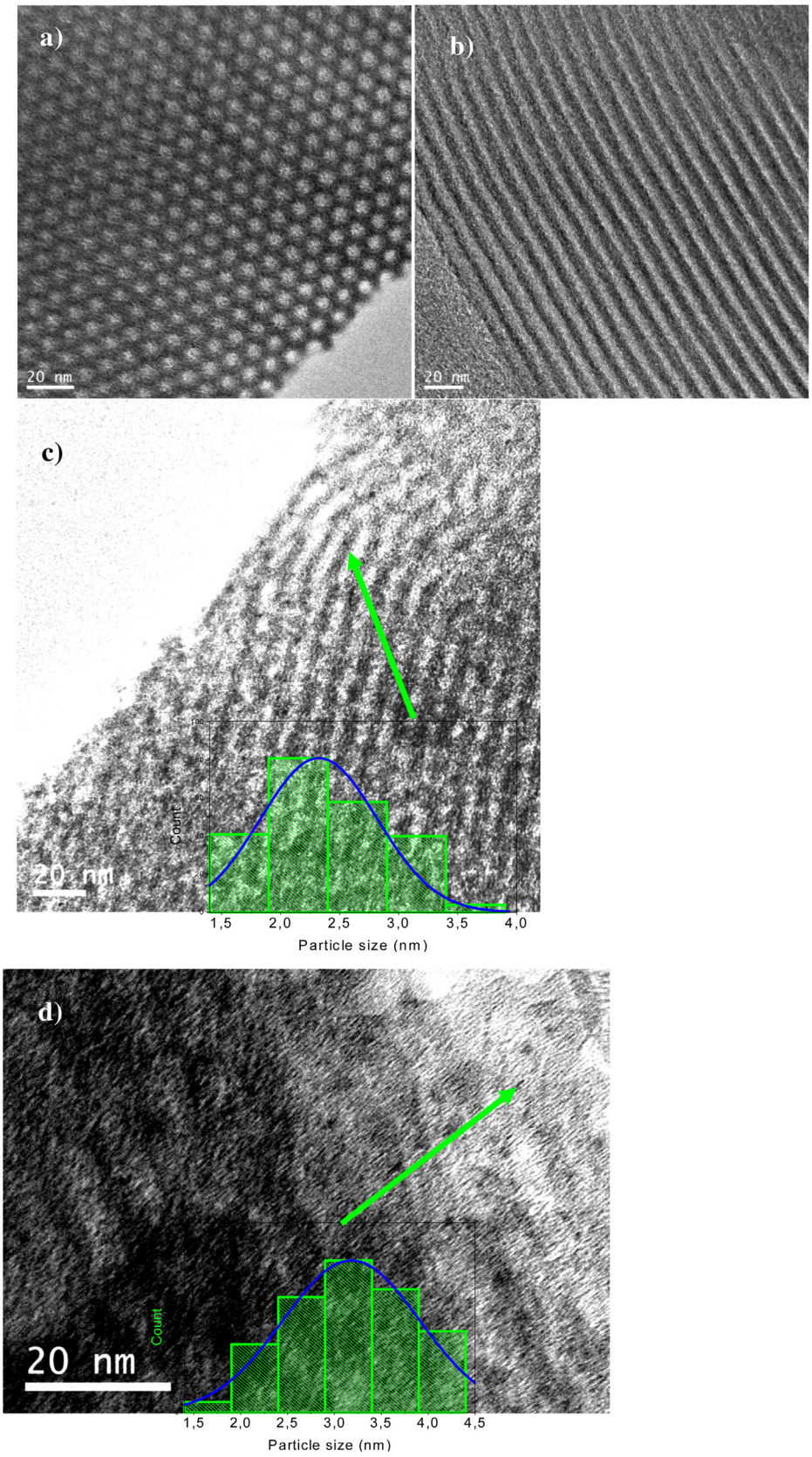


**Fig. 4.** TEM of the samples synthesized. a and (b) Ti-SBA-15; (c) Pt/Ti-SBA-15; (d) Pt-Ir-Ti-SBA-15.

**Table 4**
Kinetics constants for the different samples derived from the kinetics analysis.

| Samples | Kinetic Constant $k$ ($min^{-1}$) | Adsorption Constant $K_N$ (L/mmol) Quinoline/Indole |
|---|---|---|
| Pt-Ir/Ti-SBA-15 | 0.0325 | 145/110 |
| Pt/Ti-SBA-15 | 0.0256 | 158/130 |
| NiMo/$Al_2O_3$(Criterion DN200) | 0.0016 | 80/105 |

F = 1.56 × 10-5.

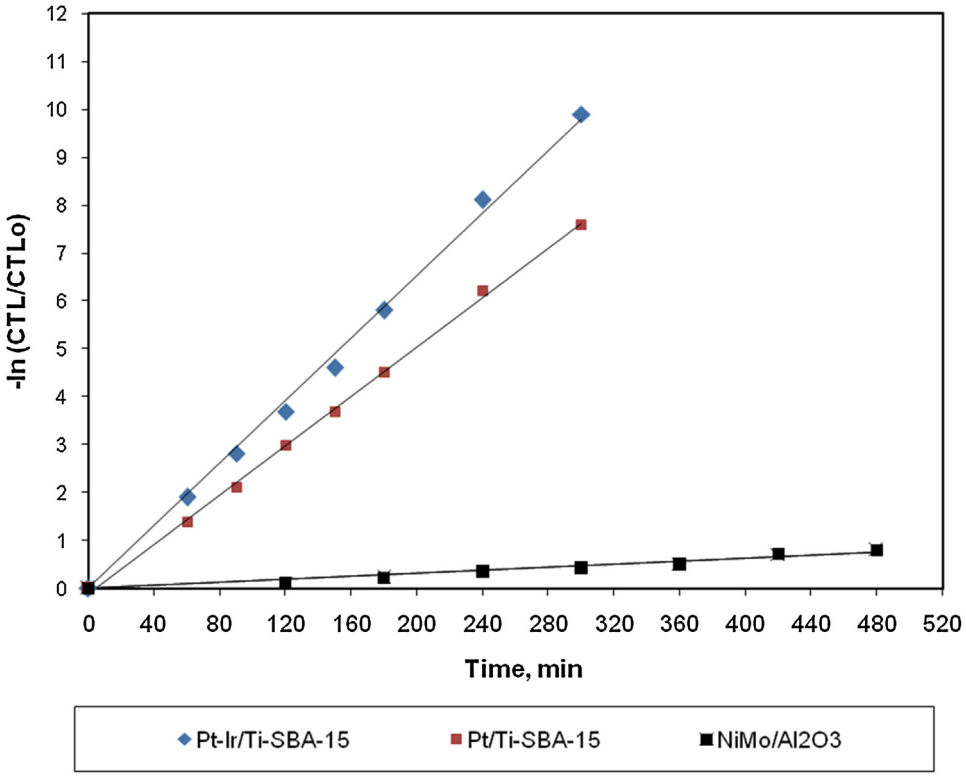


**Fig. 5.** First-order behavior of the tetralin hydrogenation without inhibitors at 250 °C and 15 atm.

### 3.2. Py-FTIR spectroscopy

The acid strength of the Ti-SBA-15 support and monometallic and bimetallic samples was studied using the pyridine adsorption method. Py-FTIR spectra of the samples were measured in the region of 1700–1400 $cm^{-1}$. Results are shown in Table 3. According to the literature, pyridine adsorbed on Lewis acid sites exhibits signals at 1450, 1596 and 1615 $cm^{-1}$ [68]. Bands at 1540 and 1640 $cm^{-1}$ are assigned to Bronsted acid sites present in the material. Further, pyridine co-adsorbed on both Bronsted and Lewis acid sites gives rise to a band at 1495 $cm^{-1}$ [69]. Py-FTIR results show that the incorporation of Ti into the framework of SBA-15 provides Lewis acidity to the catalyst. All catalysts exhibited Lewis acid sites.

### 3.3. Catalytic activity

The major products in the hydrogenation reactions of tetralin were *trans*-decalin and *cis*-decalin, the presence of naphthalene was negligible since the experiments were performed far below the thermodynamic equilibrium. Decalins appeared to be unreactive under these conditions. In order to study the behavior of the samples, computation of kinetic parameters can be useful to shed further light on this issue.

### 3.4. Kinetic model for tetralin hydrogenation in absence of inhibitors

Under the conditions of the present study, all the reactions were considered irreversible, and since hydrogen is in excess, hydrogen partial pressure was considered constant; therefore, the resulting parameters were defined as apparent. The experimental data obtained for the hydrogenation of tetralin without inhibitors in the feed were fitted to a pseudo-first-order rate equation Eq. (2) were:

$$\ln\left(\frac{Ct}{Co}\right) = -kt \quad (2)$$

Where, $k$ is the rate constant; $C_0$ (M) and Ct (M) are the concentrations of tetralin at 0 min and t min, respectively. Plots of ln ($Ct/C_0$) versus reaction time (t) are shown in Fig. 5; the linear relationships obtained, with $R^2 > 0.99$ in all the cases, confirm the pseudo-first-order reaction kinetics proposed. The catalytic results revealed a good performance of both catalysts. However, the higher rate constant was obtained for Pt-Ir/Ti-SBA-15 (Table 4).

To obtain a high selectivity to *cis*-decalin is an important goal in this work. The trans/cis ratio was found to be practically constant with the conversion for both catalysts and close to 0.6. This behavior is different for a commercial NiMo catalyst, where the trans/cis ratio are much higher and increases as the conversion increases

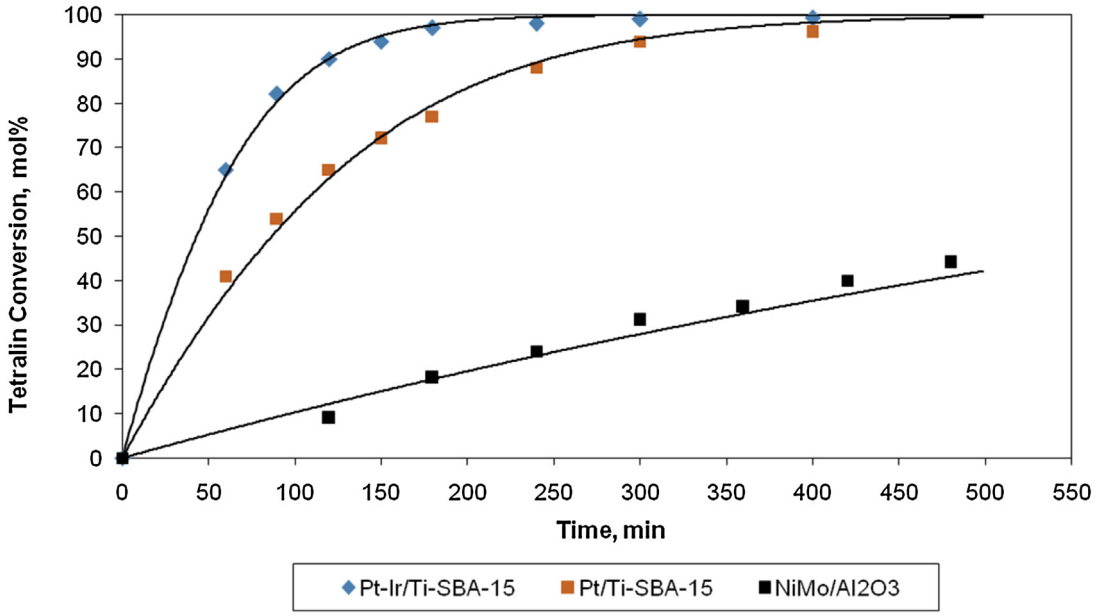


**Fig. 6.** Kinetic of the hydrogenation of tetralin at T = 250 °C, P = 15 atm, 500 rpm. Feed 1: 5 wt.% of tetralin and 150 ppm of nitrogen as indole in dodecane. The lines were obtained by fitting the kinetic curves derived from the model to the experimental data.

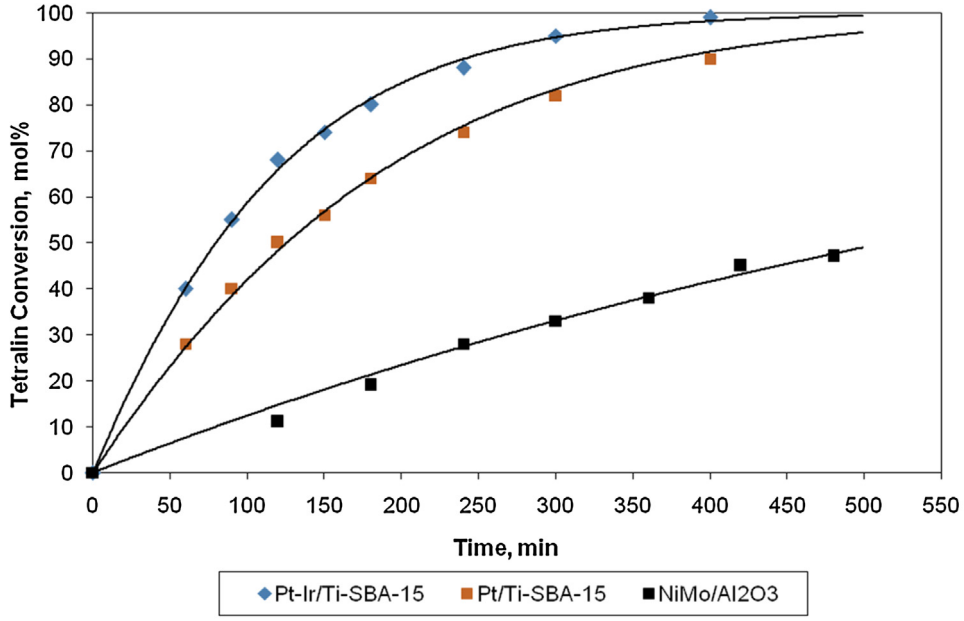


**Fig. 7.** Kinetic of the hydrogenation of tetralin at T = 250 °C, P = 15 atm, 500 rpm. Feed 2: 5 wt.% of tetralin and 150 ppm of nitrogen as quinoline in dodecane. The lines were obtained by fitting the kinetic curves derived from the model to the experimental data.

**Table 5**
Turn over frequency (TOF) of the catalysts calculated according CO chemisorptions results.

| Catalyst | CO[a] ($cm^3$/g) | D[a] (%) | TL Conversion (%)[b] Feed 1; Feed 2 | (TL moles $g^{-1}$ $min^{-1}$)[c] Feed 1; Feed 2 | TOF ($min^{-1}$) Feed 1; Feed 2 |
|---|---|---|---|---|---|
| Pt-Ir/Ti-SBA-15 | 1.32 | 72 | 98; 80 | 1.81; 1.477 | 30.7; 25.1 |
| Pt/Ti-SBA-15 | 1.45 | 78 | 77; 63 | 1.12; 0.916 | 17.3; 14.1 |

[a] Dispersion determined by CO chemisorption.
[b] Tetralin (TL) conversion at 3 h of reaction time (initial tetralin/catalyst ratio = 0.056 mol/g).
[c] Moles of tetralin converted obtained from multiply 0.056 × Conversion/100 × *k*.

**Table 6**
Atomic surface ratios of Pt-Ir/Ti-SBA-15 after three catalytic cycles obtained by XPS.

| Sample | Atomic surface ratios | | |
|---|---|---|---|
| Pt-Ir/Ti-SBA-15 | Ti/Si<br>0.0024 | Pt/Si<br>0.00074 | Ir/Si<br>0.00052 |

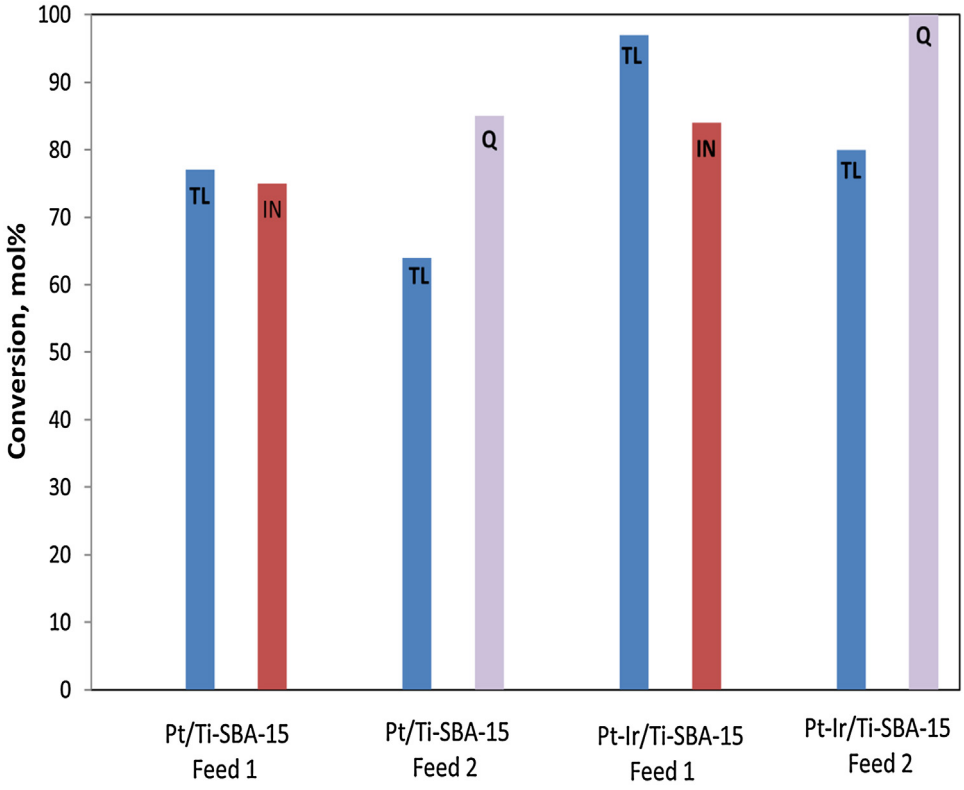


**Fig. 8.** Catalytic activity of the samples in the hydrogenation of tetralin and HDN of indole (Feed 1) and quinoline (Feed 2) at 3 h of reaction time.

[50,54,55]. We obtained high yield to *cis*-decalin, which could be further opened to form products with a high cetane number in the Ring Opening reactions [70]. As we demonstrated in previous works [50,51] iridium is selective for *cis*-decalin, and platinum is very active for hydrogenation.

### 3.5. Kinetic model for tetralin inhibition by nitrogen

The experimental data obtained for the hydrogenation of tetralin, when quinoline or indole was added in the feed, were fitted

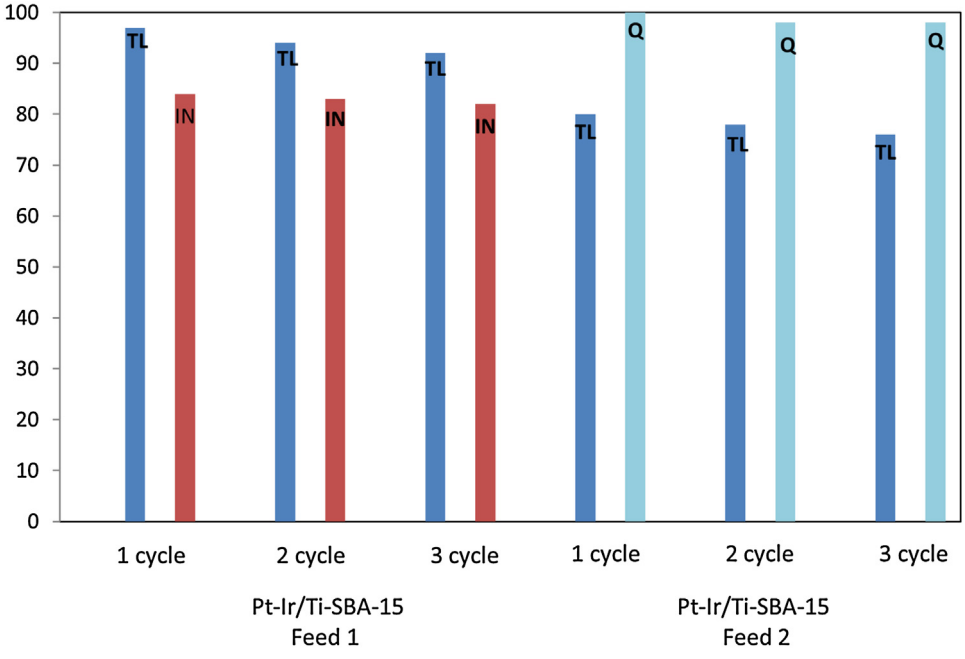


**Fig. 9.** Catalytic activity of the samples after three catalytic cycles. Cat = 250 mg, time of reaction = 3 h.

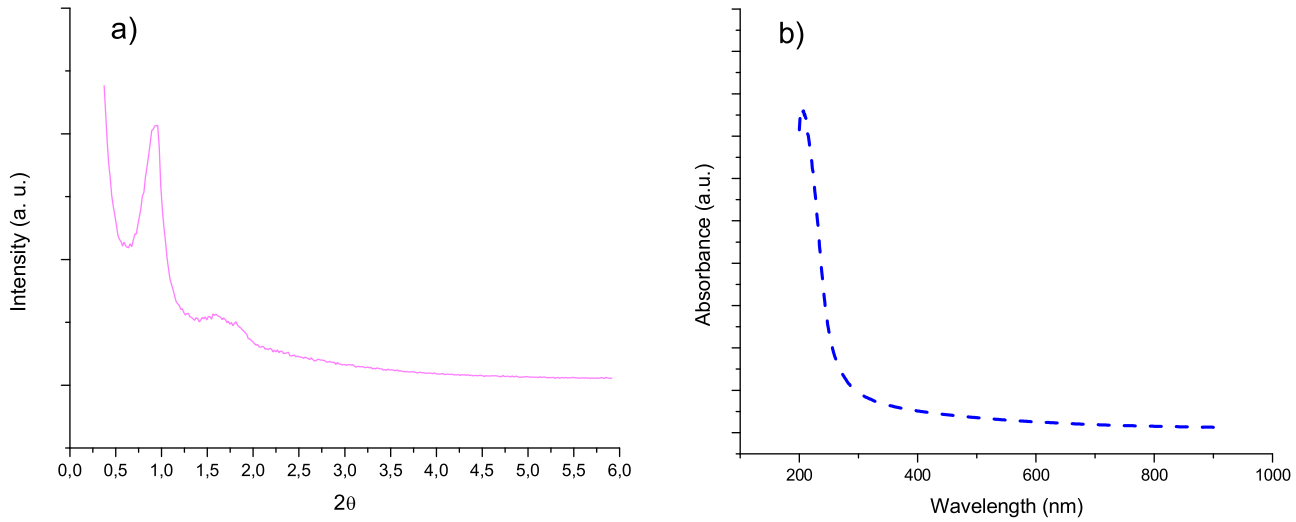


**Fig. 10.** Characterization of Pt-Ir/Ti-SBA-15 after three catalytic cycles: (a) XRD; (b) UV-VIS-DRS.

with the following equation, suggested by La Vopa and Satterfield [71]:

$$r_{TL} = \frac{k\,C_{TL}}{1 + \sum K_N C_N} \tag{3}$$

where $r_{TL}$ is the rate for the hydrogenation of tetralin inhibited by nitrogen compounds, $k$ is the pseudo-first order rate constant for the hydrogenation of tetralin with no inhibitors obtained with Eq. (2) (first column Table 4), $K_N$ is the apparent nitrogen compound adsorption equilibrium constant (L/mmol) representing the behavior of the nitrogen compound that contributes to the inhibition, and $C_N$ is the initial quinoline or indole concentration (mmol/L). The results of these experiments were fitted according to Eq. (3). The parameter estimation of the kinetic model was performed with the Powell version of the Levenberg-Marquardt algorithm. The differential equation was solved using the EPISODE package of Scientist®. The objective function Eq. (4) was the sum of the squares of the differences between experimental and calculated conversion of tetralin vs. time of the reaction, for each catalyst.

$$F = \sum_{1}^{n} \left(x_{\exp} - x_{cal}\right)^2 \tag{4}$$

The kinetics constants for the different samples derived from the kinetics analysis and the objective function value are shown in Table 4.

In this model, as a first approximation, we consider the global effect of the nitrogen compound as an inhibitor or poison, so the value of the concentration of quinoline or indole was considered constant during the reaction and equal to the initial concentration. This model does not take into account if the compound is converted or not. In fact it is known that indole or quinoline intermediates, as well ammonia has different adsorption constant depending on the characteristic surface of the catalyst. In a previous work we study the mechanism of indole HDN and determined the adsorption constant of each intermediate of indole HDN over a similar noble metal catalyst [72]. But in the case of this study the only purpose was evaluate the effect of inhibition in the hydrogenation of tetralin.

The good representation of the experimental results by the proposed rate equation implies that the inhibition effect is approximately constant during each test (Figs. 6 and 7).

The titanium-modified monometallic and bimetallic samples presented higher rates than the commercial NiMo catalyst. Pt-Ir/Ti-SBA-15 had the highest constant rate, taking into account the highest value of $k$. Quinoline presented the higher inhibiting strength in the metallic catalysts. Contrary behavior was observed with the commercial NiMo catalyst.

The good fitting of the proposed model suggests that the coverage of active sites by nitrogen compounds is established in the early stages of the reaction and remains nearly constant throughout the experiment, probably due to the slow kinetics of desorption of these compounds. As proposed by Jian and Prins [73] for the HDN of quinoline, the hydrogenated compounds could remain adsorbed and subsequently be readily transformed into products. These adsorbed species could be responsible for the inhibiting effects.

In addition, significant inhibition from $NH_3$ has been reported in some previous studies over NiMo catalyst [54,55,74,75]. In contrast, Satterfield et al. [71,76] found that $NH_3$ had no significant effect on the phenanthrene hydrogenation network until the HDN reactions were nearly complete. In a previous study, Lee and Satterfield [75] have shown that $NH_3$ can inhibit the hydrogenation of tetralin to decalins. Likewise Chadwick and Siewe [77] also found that the presence of $NH_3$ significantly reduced the rate constant (80% reduction) for tetralin hydrogenation over P-NiMo/alumina catalyst. Despite the strong influence, the effect of $NH_3$ was found to be reversible at the studied conditions. Mignard et al. [78], who studied the effect of $H_2S$ and $NH_3$ on aromatics hydrogenation over sulfided Pt and NiMo based hydrotreating catalysts, also found inhibition with ammonia. In another study, Korre [79] found that the ammonia adsorption constant was much higher than the phenanthrene adsorption constant. Although, has been no systematic study comparing its relative effect with other nitrogen compounds for the HYD and HDS reaction for noble metal catalyst.

Basic and non-basic nitrogen compounds have distinct electronic structures and properties that determine their differences in HDN reactivity on catalyst surfaces. On a catalyst with acidic surface, basic nitrogen compounds (quinoline) may show higher reactivity. In our best catalyst quinoline is further adsorbed competing with tetralin for the same sites, which could be the reason of its higher inhibition effect.

As we demonstrated above, the kinetic model described very well the inhibition effect of N-compound over tetralin hydrogenation, but in this section is interesting to note that our catalysts not only are resistant to nitrogen but also they are very active for denitrogenation reaction.

In Fig. 8 we show the conversion of tetralin and the inhibitors at 3 h of reaction time. In the figure we can see that quinoline and indole adsorption is in fact not irreversible and they are fully converted to denitrogenated products (HDN conversion defined

as mol% of denitrogenated products respect the initial concentration of the N-compound at 3 h of reaction time). We can also observe in Fig. 8, that HDN of the nitrogen-compound is very high for both catalyst and quinoline inhibition on tetralin conversion is higher than indole inhibition as determined in the kinetic study. Literature on indole HDN suggests that o-ethylaniline (OEA) is the exclusive intermediate towards formation of hydrocarbons [80–84], following indoline formation. Two major pathways were proposed to account for the formation of ethylcyclohexane (ECH) and ethylbenzene (EB), which are the two main HDN products from indole. One route occurs from hydrogenolysis of indoline (HIN) to o-ethylaniline (OEA) and the other from hydrogenation of indoline to octahydro-indole. A secondary route from o-ethylcyclohexylamine (OECHA) to ethylcyclohexene (ECHE) is also included in the mechanism proposed, occurring through a nucleophilic substitution reaction [85–88]. In this work, the products identified by GC/MS were indoline (HIN), o-ethylaniline(OEA), ethylbenzene (EB) and ethylcyclohexane (ECH); these accounted for more than 95% of the total of the products. In quinoline HDN reported studies [89–94], quinoline is hydrogenated to 1,2,3,4-tetrahydroquinoline (THQ), which subsequently undergoes C—N bond hydrogenolysis to form 2-propylaniline (OPA) and then propylbenzene, which is fully hydrogenated to propyl cyclohexane. The products identified here by GC/MS were 1,2,3,4-tetrahydroquinoline (THQ), o-propylaniline (OPA) and propylcyclohexane accounting for more than 90%.

In this work, the higher activity of the synthesized catalysts could be also related to the acidity of the support. The incorporation of tetrahedral titanium increases the Lewis acidy of the catalyst, both metallic and bimetallic samples possess Lewis acid sites (Table 3), in Pt-Ir/Ti-SBA-15 they are slightly weak, only a few of them are present at 200 °C and disappear at 300 °C. Since both catalysts are active, noble metallic sites and Lewis acid sites are believed to play an important role in the catalytic activity of Pt-Ir/Ti-SBA-15. This reinforces the idea that Lewis acidity helps for the higher HDN (C—N bond cleavage) activity. This also demonstrated the great influence of the support over the metal actives species. It can be attributed to the presence of Lewis sites derived from Ti incorporation into the framework and the effect of the support changing the electronic environment of the platinum and platinum-iridium sites. This indicates that titanium incorporation promotes HDN of indole and quinoline as was demonstrated in or previous work [72].

Previous results using $NiMo/Al_2O_3$ showed that C—N bond cleavage reactions were relatively slow compared to hydrogenation reactions under the conditions studied [88]. In the case of our best catalyst, both hydrogenation and C—N bond cleavage were very fast compared with those of NiMo catalyst. This fact could be ascribed to the high hydrogenation capacity of platinum and high hydrogenolysis capacity of iridium combined with Lewis acidity generated by the presence of titanium in the mesoporous framework. Hydrogenolysis reactions have higher activation energies than those of hydrogenation reactions and, the increase of the acidity will preferentially increase the rate of C—N bond cleavage reactions. Titanium incorporation increases hydrogenation activity compared with the PtIr-bimetallic catalyst without titanium studied in a previous work [51]. Indole and quinoline inhibition was highly decreased with the presence of titanium. Titanium allows better dispersion and good reducibility of iridium and platinum, combined with higher acidity of the support, which yields a more active catalyst.

In order to find out if there is a direct correlation between noble metal particles dispersion and activity is interesting to analyze the activity comparing the turnover frequency (TOF). For that reason, carbon monoxide chemisorptions were performed for the synthesized catalyst. Dispersion was calculated assuming a 1:1 CO to metal stoichiometry and the results are presented in Table 5. Corresponding turnover frequencies (TOF) were calculated using the number of active sites of the catalysts determined by carbon monoxide chemisorption and the converted moles of tetralin to decalin at 3 h of reaction time.

When the TOF is considered maximum activity was found with Pt-Ir/Ti-SBA-15. The different values of TOF suggest, that the higher conversion levels are more related to the nature of the catalytic centers involved in the reaction than to the particles dispersion. The higher value of TOF for Pt-Ir/Ti-SBA-15 compared with Pt/Ti-SBA-15, despite of it slight lower dispersion is evidence than the bimetallic sites are different and more active than monometallic platinum. Lower TOF were obtained when quinoline was present (Feed 2) confirming quinoline is a stronger inhibitor than indole for both catalysts.

### 3.6. Deactivation of the catalyst

The deactivation of a catalyst is very important for industrial feasibility. The reusability of the catalyst has been tested after washing with water-methanol and calcination for 2 h in a muffle furnace at 500 °C and reduced in $H_2$ flow of 20 mL/min at 470 °C using the same procedure described above. We observed that the activity remains after the third recycle for both feeds, compared to a fresh catalyst (Fig. 9). The catalysts used after 3 operation cycles were analyzed by XRD, UV–vis-DRS (Fig. 10) and XPS (Table 6) showing that the catalysts retain its structure and no leaching of Ti takes place. The reusability of the catalyst indicates that Pt-Ir/Ti-SBA-15 is a potential catalyst, which can be applied to this process.

## 4. Conclusion

The bimetallic catalyst prepared using the titanium-modified SBA-15 support was very active for HYD of tetralin and HDN of indole and quinoline. Quinoline, a basic compound, presented the higher inhibiting strength in the metallic catalysts. Contrary behavior was observed with the commercial NiMo catalyst. The dramatically difference in activity of the bimetallic-catalyst compared to the commercial $NiMo/Al_2O_3$ justify the cost.

## Acknowledgments

The authors are very grateful to Drs. J.L. García Fierro and J.M Campos Martin for some characterization techniques performed in ICP-CSIC, Madrid.

We thank CONICET Argentina, PIP CONICET 11220120100218CO (2013-2016) and UTN for financial assistance.

## References

[1] L. Allen, A. Suchanek, Hart's Fuel Technol. Manage. 8 (2) (1998) 14–16.
[2] A. Stanislaus, A. Marafi, M.S. Rana, Catal. Today 153 (2010) 1–68.
[3] H. Topsøe, B. Hinnemann, J.K. Nørskov, J.V. Lauritsen, F. Besenbacher, P.L. Hansen, G. Hytoft, R.G. Egeberg, K.G. Knudsen, Catal. Today 12 (2005) 107–108.
[4] T. Fujikawa, Top. Catal. 52 (2009) 872.
[5] M. Breysse, C. Geantet, P. Afanasiev, J. Blanchard, M. Vrinat, Catal. Today 130 (2008) 3.
[6] K. Segawa, K. Takahashi, S. Satoh, Catal. Today 63 (2000) 123.
[7] V. Costa, K. Marchand, M. Digne, C. Geantet, Catal. Today 130 (2008) 69.
[8] N. Frizi, P. Blanchard, E. Payen, P. Baranek, C. Lancelot, M. Rebeilleau, C. Dupuy, J.P. Dath, Catal. Today 130 (2008) 32.
[9] S.T. Oyama, T. Gott, H. Zhao, Y.-K. Lee, Catal. Today 143 (2009) 94.
[10] K.G. Knudsen, B.H. Cooper, H. Topsoe, Appl. Catal. A: Gen. 189 (1999) 205–215.
[11] B.H. Cooper, K.G. Knudsen, Practical Advances in Petroleum Processing, Book Chapter 10, 2006, pp. 297.
[12] R.R. Bharvani, R.S. Henderson, Hydrocarb. Process. 81 (2002) 61–64.
[13] A. Marafi, A. Al-Hindi, A. Stanislaus, Fuel Process. Technol. 88 (2007) 905–911.
[14] T.C. Ho, Appl. Catal. A: Gen. 244 (2003) 115–128.
[15] S. Torrisi, P.M. Gunter, NPRA Annual Meeting (2004).
[16] T.C. Ho, Catal. Today 98 (2004) 3–18.

[17] X. Ma, K. Sakarishi, T. Isoda, I. Mochida, Ind. Eng. Chem. Res. 33 (1994) 218–222.
[18] M. Houalla, D.H. Broderick, A.V. Spare, N.K. Nag, V.H.J. De Beer, B.C. Gates, J. Catal. 61 (1980) 523–527.
[19] H. Schulz, W. Bohringer, P. Waller, F. Ousmanov, Catal. Today 49 (1999) 87–97.
[20] M. Egorova, R. Prins, J. Catal. 225 (2004) 417–427.
[21] H. Farag, K. Sakanishi, M. Kouzu, A. Matsumura, Y. Sugimoto, I. Saito, Ind. Eng. Chem. Res. 42 (2003) 306–310.
[22] J. Leglise, J.N.M. Van Gestel, L. Finot, J.C. Duchet, J.L. Dubois, Catal. Today 45 (1998) 347–352.
[23] V. Rabarihoela-Rakotovao, S. Brunet, G. Perot, F. Diehl, Appl. Catal. A: Gen. 306 (2006) 34–44.
[24] H. Farag, Appl. Catal. A: Gen. 331 (2007) 51–59.
[25] P. Zeuthen, K.G. Knudsen, D.D. Whitehurst, Catal. Today 65 (2001) 307–314.
[26] K.H. Choi, Y. Korai, I. Mochida, I.W. Ryu, W. Min, Appl. Catal. B: Environ. 50 (2004) 9–16.
[27] U.T. Turaga, X.L. Ma, C.S. Song, Catal. Today 86 (2003) 265.
[28] V. Rabarihoela-Rakotovao, F. Diehl, S. Brunet, Catal. Lett. 129 (2009) 50–56.
[29] Z. Liu, Q. Zhang, Y. Zheng, J. Chen, Energy Fuels 22 (2008) 860–866.
[30] T. Song, Z. Zhang, J. Chen, Z. Ring, H. Yang, Y. Zheng, Energy Fuels 20 (2006) 2344–2349.
[31] P. Steiner, Doctorate Thesis, The Norwegian University of Science and Technology, Department of Chem. Eng., 2002.
[32] H. Farag, K. Sakanishi, I. Mochida, D.D. Whitehurst, Energy Fuels 13 (1999) 449–453.
[33] J. Cinibulk, Z. Vit, Appl. Catal. A: Gen. 204 (2000) 107.
[34] Z. Vit, J. Cinibulk, React. Kinet. Catal. Lett. 72 (2001) 189.
[35] Z. Vit, J. Cinibulk, React. Kinet. Catal. Lett. 77 (2002) 43.
[36] J. Cinibulk, Z. Vit, Stud. Surf. Sci. Catal. 143 (2002) 443.
[37] J. Cinibulk, D. Gulkova, Y. Yoshimura, Z. Vit, Appl. Catal. A: Gen. 255 (2003) 321.
[38] M.J. Dees, A.J. den Hartog, V. Ponec, Appl. Catal. 72 (1991) 343.
[39] N. Kunisada, K.H. Choi, Y. Korai, I. Mochida, K. Nakano, Appl. Catal. A: Gen. 269 (2004) 43–51.
[40] J.C. Duchet, M.J. Tilliete, D. Cornet, L. Vivier, G. Perot, L. Bekakra, C. Moreau, G. Szabo, Catal. Today 10 (1991) 579–592.
[41] J. Ramirez, S. Fuentes, G. Diaz, M. Vrinat, M. Breysse, M. Lacroix, Appl. Catal. 52 (1989) 211–224.
[42] D. Trong On, D. Desplantier-Giscard, C. Danumah, S. Kaliaguine, Appl. Catal. A: Gen. 253 (2003) 545–602.
[43] K.C. Mouli, K. Soni, A. Dalai, J. Adjaye, Appl. Catal. A: Gen. 404 (2011) 21–29.
[44] G. MuraliDhar, G.M. Kumaran, M. Kumar, K.S. Rawat, L.D. Sharma, B.D. Raju, K.S. Rama Rao, Catal. Today 99 (2005) 309–314.
[45] K. Soni, B.S. Rana, A.K. Sinha, A. Bhaumik, M. Nandi, M. Kumar, G.M. Dhar, Appl. Catal. B: Environ. 90 (2009) 55–63.
[46] S. Garg, T. Bhaskar, K. Soni, G.M. Kumaran, A. Muto, Y. Sakata, G. MuraliDhar, Chem. Commun. (2008) 5310–5311.
[47] N. Kostova, A. Spojakina, K. Jiratova, O. Solcova, L. Dimitrov, L. Petrov, Catal. Today 65 (2001) 217.
[48] O.Y. Gutierrez, D. Valencia, G.A. Fuentes, T. Klimova, J. Catal. 249 (2007) 138.
[49] G.M. Kumaran, S. Garg, K. Soni, M. Kumar, L.D. Sharma, G.M. Dhar, K.S.R. Rao, Appl. Catal. A: Gen. 305 (2006) 123.
[50] B.C. Ledesma, V.A. Vallés, L.P. Rivoira, M.L. Martinez, O.A. Anunziata, A.R. Beltramone, Catal. Lett. 144 (5) (2014) 783–795.
[51] V.A. Vallés, B.C. Ledesma, L.P. Rivoira, J. Cussa, O.A. Anunziata, A.R. Beltramone, Catal. Today 271 (2016) 140–148.
[52] S.C. Korre, M.T. Klein, R.J. Quann, Ind. Eng. Chem. Res. 34 (1995) 101–117.
[53] S. Toppinen, T. Salmi, T.K. Aittamaa, J. Ind. Eng. Chem. Res. 36 (1997) 2101–2109.
[54] A. Beltramone, S. Crossley, D. Resasco, W. Alvarez, Catal. Letters. 123 (2008) 181–185.
[55] A.R. Beltramone, D.E. Resasco, W.E. Alvarez, Ind. Eng. Chem. Res. 47 (2008) 19.
[56] V. Valles, G. Balangero Bottazzi, M. Martínez, M. Gómez Costa, O. Anunziata, A. Beltramone, Ind. Eng. Chem. Res. 51 (2012) 7185–7195.
[57] G. Petrini, A. Cesana, G.F. De Alberti, G. Genoni, M. Leofanti, M. Padovan, G. Paparatto, P. Roffia, Stud. Surf. Sci. Catal. 68 (1991) 761–766.
[58] Z. Luan, E.M. Maes, P.A.W. Van der Heide, D. Zhao, R.S. Czernuszewicz, L. Kevan, Chem. Mater. 11 (1999) 3680–3686.
[59] S.Y. Balaji, Raman Spectrosc. 37 (2006) 1416–1422.
[60] W.H. Zhang, J. Lu, B. Han, M. Li, J. Xiu, Y.P. Ying, C. Li, Chem. Mater. 14 (2002) 3413.
[61] Li Zhao, Jiagu. Yu, J. Colloid Interface Sci. 304 (2006) 84–91.
[62] V.V. Atuchin, V.G. Kesler, N.V. Pervukhina, Z. Zhang, J. Electron Spectrosc. Relat. Phenom. 152 (12) (2006) 18–24.
[63] A. Infantes-Molina, J. Merida-Robles, E. Rodriguez-Castellon, J.L.G. Fierro, A. Jimenez-Lopez, Appl. Catal. B: Environ. 73 (2007) 180–192.
[64] M. Wakisaka, S. Mitsui, Y. Hirose, K. Kawashima, H. Uchida, M. Watanabe, J. Phys. Chem. B 110 (2006) 46.
[65] I. Radev, G. Topalov, E. Lefterova, G. Ganske, U. Schnakenberg, G. Tsotridis, et al., Int. J. Hydrogen Energy 37 (2012) 9.
[66] I.H. Sinfelt, Bimetallic catalysts: discoveries concepts, and applications, in: Exxon Monographs Series, John Wiley, New York, 1983.
[67] S. Subramanian, J.A. Schwarz, Appl. Catal. 6 (1991) 74.
[68] E. Barzetti, D. Selli, J. Chem. Soc. Faraday Trans. 92 (1996) 1401–1407.
[69] T.R. Hughes, H.M. White, J. Phys. Chem. 71 (1967) 2192–2201.
[70] A.W. Weitkamp, Adv. Catal. 18 (1968) 1.
[71] V. LaVopa, C.N. Satterfield, J. Catal. 110 (1988) 375–387.
[72] B.C. Ledesma, O.A. Anunziata, A.R. Beltramone, Appl. Catal. B: Env. 192 (2016) 220–233.
[73] M. Jian, R. Prins, J. Catal. 179 (1998) 18.
[74] M.J. Girgis, B.C. Gates, Ind. Eng. Chem. Res. 30 (1991) 2021.
[75] C.M. Lee, C.N. Satterfield, Energy Fuels 6 (1992) 315–317.
[76] C.M. Lee, C.N. Satterfield, Energy Fuels 3 (1992) 978.
[77] D. Chadwick, A. Siewe, Catal. Today 29 (1996) 229.
[78] N. Mignard, Bull. Soc. Chim. Belges 104 (4–5) (1995) 259–263.
[79] S.C. Korre, PhD. Thesis, University of Delaware, 1994, 2016.
[80] F.E. Massoth, K. Balusami, J. Shabtai, J. Catal. 122 (1990) 256–270.
[81] P. Zeuthen, P. Stolze, U.B. Pedersen, Bull. Soc. Chim. Belg. 96 (1987) 985–995.
[82] J. Shabtai, G. Que, K. Balusami, N.K. Nag, F.E. Massoth, J. Catal. 113 (1988) 206–219.
[83] W.V. Steele, R.D. Chirico, Topical Report for US DOE, Fossil Energy, Contract No. 22–83FE60149, NIPER 379, 1988.
[84] J.L. Olive, S. Biyoko, C. Moulinas, P. Geneste, Appl. Catal. 19 (1985) 165–174.
[85] G.M. Kumaran, S. Garg, K. Soni, M. Kumar, L.D. Sharma, G.M. Dhar, K.S.R. Rao, Appl. Catal. A 305 (2006) 123–129.
[86] L. Zhang, U.S. Ozkan, Stud. Surf. Sci. Catal. 106 (1997) 69–82.
[87] E.O. Odebunmi, D.F. Ollis, J. Catal. 80 (1983) 76–89.
[88] A. Bunch, L. Zhang, G. Karakas, U.S. Ozkan, Appl. Catal. A 190 (2000) 51–60.
[89] M. Machida, Y. Sakao, S. Ono, Appl. Catal. A 187 (1999) L73–L78.
[90] S.H. Yang, C.N. Satterfield, J. Catal. 81 (1983) 168–178.
[91] C. Moreau, L. Bekakra, R. Durand, P. Geneste, Catal. Today 10 (1991) 681–687.
[92] S.C. Kim, J. Simons, F.E. Massoth, J. Catal. 212 (2002) 201–206.
[93] C. Liu, Y. Yu, H. Zhao, Fuel Process. Technol. 86 (2004) 449–460.
[94] S. Gultekin, M. Khaleeq, M.A. Al-Saleh, Chem. Eng. J. 46 (1991) 79–89.